

1 **Fossil-Dominated SOA Formation in Coastal China: Size-Divergent**  
2 **Pathways of Aqueous Fenton Reactions versus Gas-phase VOC**  
3 **Autoxidation**

4 Jia-Yuan Wang, Meng-Xue Tang, Shan Lu, Ke-Jin Tang, Xing Peng, Ling-Yan He, Xiao-Feng  
5 Huang

6 Key Laboratory for Urban Habitat Environmental Science and Technology, Peking University Shenzhen  
7 Graduate School, Shenzhen, 518055, China.

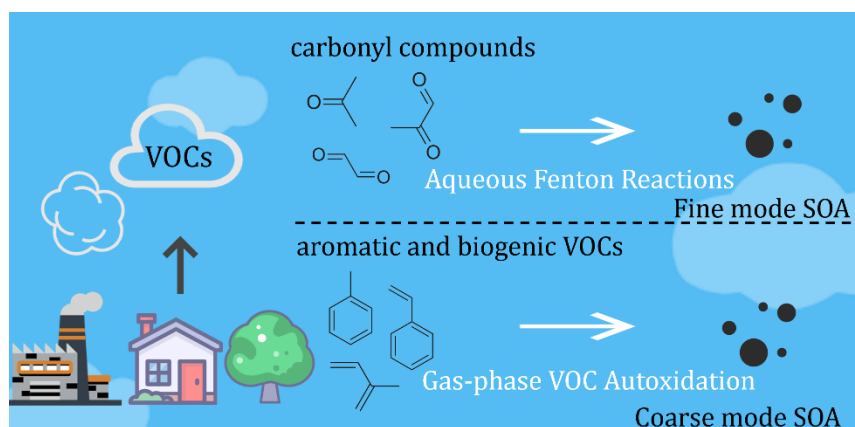
8 Corresponding author: Meng-Xue Tang ([tangmx@pku.edu.cn](mailto:tangmx@pku.edu.cn))

9

**Abstract:** Elucidating size-dependent formation mechanisms of secondary organic aerosols (SOA) remains a critical research gap in atmospheric chemistry. Here, we analyzed water-soluble compounds in size-segregated aerosol samples (0.056–18  $\mu\text{m}$ ) collected at a coastal site in southern China. Radiocarbon ( $^{14}\text{C}$ ) isotope analysis reveals that fossil sources dominate SOA in both fine (95.8%) and coarse (80.4%) modes, while the small amount of biogenic SOA mostly existed in the coarse mode (74.1%). Fine-mode oxygenated organic carbon (OOC) correlates strongly with polar carbonyl compounds (e.g., glyoxal, methylglyoxal, acetone, and MVK+MACR), while coarse-mode OOC exhibits better correlations with nonpolar aromatic hydrocarbons (e.g., toluene, C8 aromatic, C9 aromatic, styrene) and biogenic volatile organic compounds (VOCs) (e.g., monoterpenes, isoprene), indicating that the sources of fine- and coarse-mode OOC are different. Multivariate analyses incorporating inorganic ions, pH, water-soluble iron ions, aerosol liquid water content, and  $\text{O}_3$  revealed divergent size-dependent mechanisms, emphasizing the significant role of aqueous-phase reactions in fine-mode OOC formation, particularly the key contribution of water-soluble Fe ions ( $r^2 = 0.74$ ), while coarse-mode OOC exhibited a notable correlation with  $\text{O}_3$  ( $r^2 = 0.63$ ). Combining the information on VOCs precursors and key components, our study elucidates that aqueous-phase reactions play a key role in fine-mode OOC, especially the Fenton reaction, while gas-phase VOC autoxidation plays an important role in the coarse-mode OOC generation. By examining OOC formation across a wide range of particle sizes, our study highlights the critical need for mode-specific treatment of SOA generation in atmospheric chemical transport modeling.

**Key words:** Secondary organic aerosol (SOA), Fine mode, Coarse mode, Aqueous-phase reactions, Gas-phase autoxidation

32 **Graphical abstract:**



33

## 1.Introduction

In urban areas, organic aerosol (OA) constitutes 30-70% of submicron particle mass( Zhang et al., 2017b) and has significant impacts on human health, radiation balance, and air quality. OA can originate from direct emissions (primary organic aerosol, POA) or be formed in the atmosphere through the oxidation of semi-volatile and volatile organic compounds (VOCs), resulting in secondary organic aerosol (SOA)(Peng et al., 2021). Globally, SOA is estimated to contribute up to 93% of the total OA budget (Hallquist et al., 2009). However, our understanding of the SOA formation mechanisms is still limited, the complexities of SOA formation are not only due to the presence of large amounts of biogenic and anthropogenic VOC precursors, but also because each VOC can undergo a number of atmospheric degradation processes (e.g., gas-phase radical-mediated oxidation, heterogeneous oxidation, and oligomerization) to produce various condensable oxidized organics (COO) with distinct functionality, reactivity, and volatility(Gu et al., 2023; Xu et al., 2017; Yu et al., 2016).

SOA can be formed from the atmospheric oxidation of VOCs or originate from various processes such as heterogeneous reactions, photochemistry, and aqueous-phase oxidation (Dominutti et al., 2022). Field studies on SOA formation have mostly focused on fine particles ( $PM_{10}$ ), partly due to instrument limitations(Xu et al., 2017; Yao et al., 2022a). Recent mass spectrometry-based studies have suggested that photochemical oxidation is a major pathway for SOA formation, typically initiated by reactions with radicals (e.g., OH,  $NO_3$ ) or oxidants (e.g.,  $O_3$ ), producing a variety of condensable oxidized organics (COOs) that subsequently engage in gas-to-particle conversion(Xu et al., 2017; Zhan et al., 2021). However, aqueous-phase SOA formation is also an important pathway, with SOA forming on wet aerosols, clouds, and fogs through further chemical processes involving water-soluble organic compounds or the organic products of gas-phase photochemistry(Ervens et al., 2011; Gu et al., 2023; Mei

56 et al., 2025).

57 While the formation of SOA on coarse particles was mostly neglected, coarse particles (both natural  
58 and anthropogenically emitted dust) is constantly present in the atmosphere and is one of the largest  
59 contributors to aerosol mass in the troposphere(Wu et al., 2024; Xu et al., 2024), exerting a significant  
60 impact on global climate by modulating radiative balance. Coarse particles mainly consist of  
61 aluminosilicate, SiO<sub>2</sub>, CaCO<sub>3</sub>, sea salt, and coated with secondary organic and inorganic aerosol  
62 components under an ambient environment(Li and Shao, 2009; Yang et al., 2024), coarse particles act as  
63 reactants or catalysts, enhancing atmospheric heterogeneous reactions and photochemical processes(Pan  
64 et al., 2023; Wang et al., 2020b).Heterogeneous reactions and photochemical reactions on mineral dust  
65 may play an important role in coarse modal SOA generation (George et al., 2015; He et al., 2022a; Wang  
66 et al., 2020b).This also suggests that different formation mechanisms may govern fine-mode and coarse-  
67 mode secondary organic aerosols.

68 In this study, we collected a broad range of size-segregated samples (0.056-18 μm) from Shenzhen, a  
69 coastal city in southern China, to obtain comprehensive particle size information. We utilized the offline  
70 ACSM-PMF method to characterize SOA in these samples and combined it with <sup>14</sup>C analysis to gain a  
71 deeper understanding of SOA from fossil fuel and biogenic sources (He et al., 2022a; Huang et al., 2020).  
72 This study explores the mechanisms of SOA formation across both fine-mode and coarse-mode,  
73 enhancing our understanding of the diverse generation mechanisms of SOA across various particle size  
74 distributions.

## 2. Material and methods

### 2.1 Sampling site and sample collection

The sampling site, Atmospheric Observation Supersite of Shenzhen (AOSS, 22.60 °N, 113.98 °E), is located at an urban site in the southeast of the Pearl River Delta (PRD) region. There are no significant local pollution sources in the vicinity. The sampling period encompassed both the peak of particulate matter pollution and the most severe photochemical pollution in Shenzhen for the year. The levels of VOCs at this site are typically influenced by continental air masses, marine air masses, and local biogenic emissions (Li et al., 2024a). A ten-stage micro-orifice uniform deposit impactor (MOUDI, model 110, MSP Co., USA) with aerodynamic diameter cut-points of 0.056, 0.1, 0.18, 0.32, 0.56, 1.0, 1.8, 3.2, 5.6, 10, and 18  $\mu\text{m}$  was used to collect size-segregated aerosol samples on Teflon filters from 21 October 2022 to 3 February 2023. In this study, we found that 1-1.8  $\mu\text{m}$  particles showed more coarse mode properties, so we took 1  $\mu\text{m}$  as the division boundary, so we use 1  $\mu\text{m}$  as the boundary between fine particles and coarse particles, in this study. The sampling flow rate was 30 L/min. The average ambient temperature during the sampling period was 20.0 °C, and the dominant wind direction was northeasterly. In total, one hundred and sixty samples were collected with a sampling cycle of 72 hours.

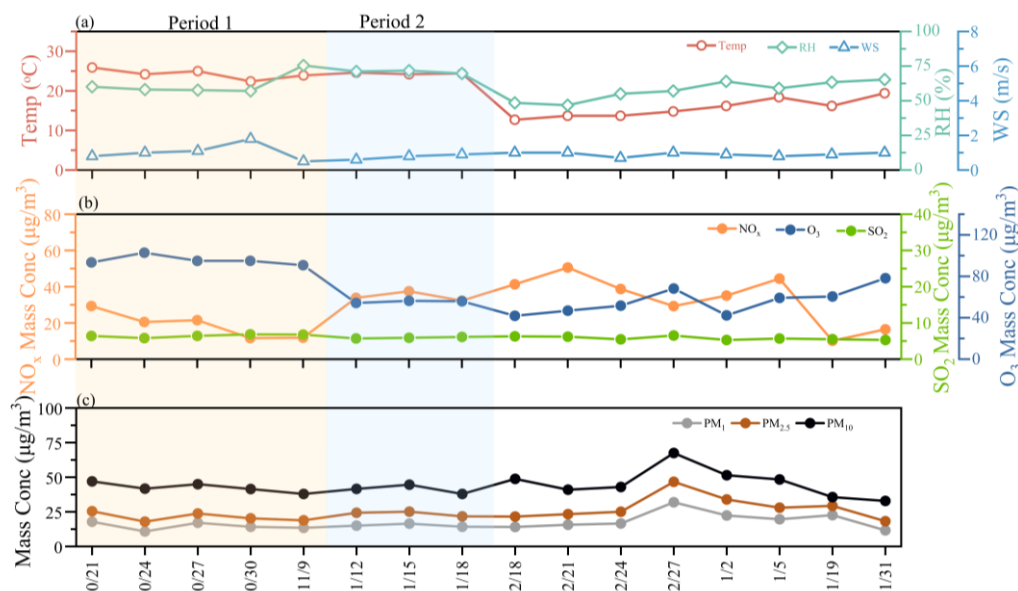


**Figure 1.** Time series of relative humidity (RH), Temperature (Temp) and wind speed (WS) (a), O<sub>3</sub>, SO<sub>2</sub> and NO<sub>x</sub> (b), PM<sub>1</sub>, PM<sub>2.5</sub> and PM<sub>10</sub> (c). The time series were categorized to be two typical periods based on total O<sub>3</sub> mass concentrations: the high-O<sub>3</sub> period (Period 1), and the low-O<sub>3</sub> period (Period 2).

## 2.2. Chemical analysis

The mass of the size-segregated aerosol samples was obtained from the difference in mass of the Teflon filter before and after sampling in a cleanroom at conditions of 22.1 °C and 49.2% relative humidity. Then, each filter was extracted with 20 mL of ultrapure water in an ultrasonic bath with ice for 30 min and then filtered with a 0.22 µm Teflon filter for further analysis. A portion of the water extract was analyzed for water-soluble metal elements using an inductively coupled plasma mass spectrometer (ICP-MS, Bruker auroraM90, Germany). Inorganic ions ( $\text{Cl}^-$ ,  $\text{SO}_4^{2-}$ ,  $\text{NO}_3^-$ ,  $\text{NH}_4^+$ ,  $\text{Na}^+$ ,  $\text{K}^+$ ,  $\text{Mg}^{2+}$ ,  $\text{Ca}^{2+}$ ) were measured using an ion chromatography system (ICS-6000, Dionex, USA). A portion was analyzed for water-soluble organic matter (WSOM) and the corresponding mass spectra using a Nebulizer-ACSM system (ToF-ACSM-X, Aerodyne Research, Inc., USA) and a portion was analyzed for water-soluble organic carbon (WSOC) with a total organic carbon analyzer (N/C 3100, Analytik Jena AG, Germany) to quantify organic oxygen (WSOO, WSOM), the major ion fragments ( $m/z$  44,  $m/z$  57,  $m/z$  56,  $m/z$  58) and elements (C, H, O, and N) measured by ToF-ACSM-X. Equal amounts of the water extract from the same MOUDI stages were combined and concentrated for  $^{14}\text{C}$  analysis based on accelerator mass spectrometry. More details of the Nebulizer-ACSM and radiocarbon can be found in (He et al., 2022a; Huang et al., 2020).

## 2.3 Other measurements

A meteorological monitoring instrument (WXT536, Vaisala, Finland) was used to measure the meteorological variables, including atmospheric temperature (Temp), relative humidity (RH), wind direction (WD), and wind speed (WS). Criteria air pollutants were monitored using the following instruments: a 5030i  $\text{PM}_{2.5}$  and 5030i  $\text{PM}_{10}$  for particulate matter, a 43i  $\text{SO}_2$  analyzer, a 42i  $\text{NO}_x$  analyzer, a 49i  $\text{O}_3$  analyzer, and a 48i CO analyzer (Thermo Scientific, USA). Additionally, PTR-ToF-MS (6000X2,

Ionicon Analytik GmbH, Austria) with  $\text{H}_3\text{O}^+$  ionization mode was used for online measurements of volatile organic compounds at the same site during the campaign. Further details regarding the PTR-ToF-MS are available in (He et al., 2022b; Li et al., 2024b).

## 2.4 Data analysis

The inorganic ion components of size-segregated aerosol samples ( $\text{Cl}^-$ ,  $\text{SO}_4^{2-}$ ,  $\text{NO}_3^-$ ,  $\text{Na}^+$ ,  $\text{NH}_4^+$ ,  $\text{K}^+$ ,  $\text{Mg}^{2+}$ ,  $\text{Ca}^{2+}$ ), along with relative humidity (RH) and temperature were input into ISORROPIA II model to calculate the aerosol liquid water content (ALWC) and aerosol pH ( $\text{pH}_{\text{aerosol}}$ ), the thermodynamic equilibrium model ISORROPIA II was used to estimate the size-resolved ALWC and  $\text{pH}_{\text{aerosol}}$  in this study owing to its accuracy, reliability, and high computational efficiency (Duan et al., 2020; Tan et al., 2017; Xu et al., 2024). The Pearson correlation method was applied using SPSS Statistics software for correlation analysis. Quantitative source apportionment of water-soluble organic carbon (WSOC) was conducted with the U.S. EPA PMF v5.0 software. Data matrices and error matrix of WSOC, WSOO,  $\text{CO}_2^+$ ,  $\text{C}_4\text{H}_9^+$ , and  $\text{nss-K}^+$  for a total of 160 samples (16 sets  $\times$  10 stages) were input into the PMF model, the three-factor (the more oxidized oxygenated organic carbon (MO-OOC), the less oxidized OOC (LO-OOC), and biomass-burning organic carbon (BBOC) determined to be the most reasonable solution (Figure S1). More details of the source apportionment of WSOC by PMF modeling are provided in the supporting information. Considering the significant contribution of sea salt at the sampling site, non-sea-salt potassium ( $\text{nss-K}^+$ ) was calculated to better represent biomass burning emissions.  $\text{Nss-K}^+$  was calculated from measured  $\text{K}^+$  assuming the mass ratio  $\text{K}^+/\text{Na}^+$  of 0.036 as in seawater, following the approach in (Boreddy and Kawamura, 2015; Klopper et al., 2020).



### 3 Results and discussion

#### 3.1 average size distributions of the aerosol components

Figure 2a shows the average size distributions of the aerosol components, coarse modes exhibit higher mass concentrations, accounting for 66.7% of the total mass. The coarse mode contains significantly higher proportions of water-insoluble components, with measured concentrations reaching  $20.63 \mu\text{g m}^{-3}$ , accounting for 75.6% of the total coarse-mode mass concentration. Unlike the coarse mode, the fine mode has a higher proportion of water-soluble components. As is shown in Figure 2b, the main water-soluble inorganic ions in the fine mode differ from those in the coarse mode, sulfate ( $\text{SO}_4^{2-}$ ) and ammonium ( $\text{NH}_4^+$ ) are the most abundant compounds in the fine mode, constituting 17.0% and 7.4% of the total mass of fine particles, respectively. In contrast, nitrate ( $\text{NO}_3^-$ ) and calcium ( $\text{Ca}^{2+}$ ) are the predominant inorganic ions in the coarse mode, comprising 5.6% and 1.5% of the total mass of coarse particles, respectively. Although the compositions of fine- and coarse-mode water-soluble inorganic ions differ significantly, water-soluble organic matter (WSOM) is the most abundant water-soluble component in both modes. WSOM constitutes 55.9% of the total water-soluble mass in fine particles and 40.9% in coarse particles, underscoring its critical role in both size modes.

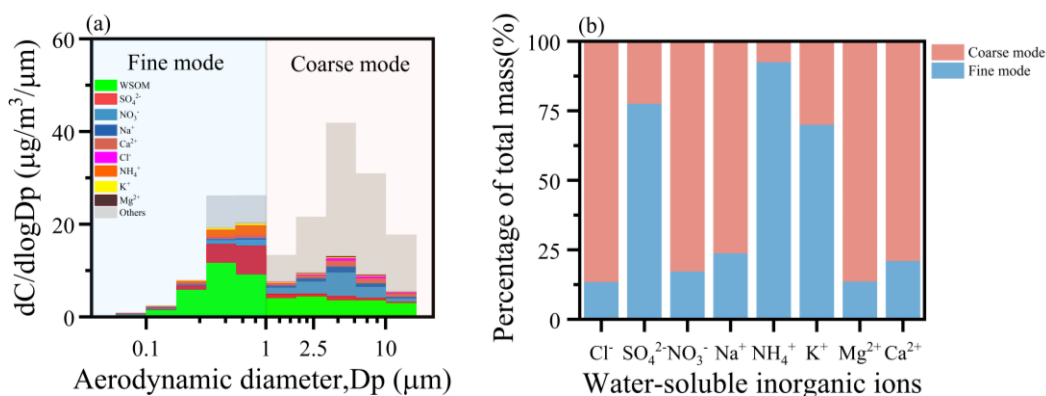


**Figure 2.** The average size distributions of aerosol components at this site (a), the percentage of the fine mode and coarse mode of water-soluble inorganic ions (b). The “others” category was calculated by the mass concentration of particulate matter minus the total concentrations of water soluble species, and might include non-water soluble organic matter, elemental carbon, crustal material, etc.

### 3.2 Possible sources of fine and coarse mode SOA

In this study, PMF is used to extract OA components. The three-factor solution was considered the most reasonable based on the clarity of factor profiles and the residual distribution. Further details are provided in the Supplement. Figure 3a presents the contributions of Oxygenated Organic Carbon (OOC), defined as the sum of MO-OOC (moderately oxygenated organic carbon) and LO-OOC (lowly oxygenated organic carbon), as well as Biomass Burning Organic Carbon (BBOC), across all particle size bins. The results indicate that BBOC was mainly disturbed in the fine mode accounting for 91.1% of the total BBOC. OOC dominated in both the fine (64.4%) and coarse mode (88.4%), and previous studies found that the fine mode SOA can be estimated by WSOC after removing the contribution of biomass burning (He et al., 2022b; Huang et al., 2020), in this study, OOC is equivalent to SOA. This highlights the critical role of SOA in both the fine and coarse mode.

Figure 3b shows the size distributions of fossil fuel OOC and biogenic OOC in all size bins, which

were calculated by combining the results from the PMF factor contributions and the  $^{14}\text{C}$  isotope analysis, and the calculations were performed as in our previous study with equations (1)-(3) (He et al., 2022a; Huang et al., 2020) :

$$\text{biogenic carbon} = \text{WSOC} * f_{\text{modern}} \quad (1)$$

$$\text{biogenic OOC} = \text{biogenic carbon} - \text{BBOC} \quad (2)$$

$$\text{fossil fuel OOC} = \text{OOC} - \text{biogenic OOC} \quad (3)$$

Here,  $f_{\text{modern}}$  represents the modern carbon fraction, defined as the ratio of the  $^{14}\text{C}/^{12}\text{C}$  content in a sample relative to that of a modern standard (NBS Oxalic Acid I from AD 1950), corrected for  $\delta^{13}\text{C}$  isotopic fractionation and  $^{14}\text{C}$  decay (Zhang et al., 2019). Biogenic carbon represents the portion of carbon derived from biogenic sources, biogenic OOC represents the oxygenated organic carbon originating from biogenic sources, fossil fuel OOC represents the oxygenated organic carbon derived from fossil fuel sources.

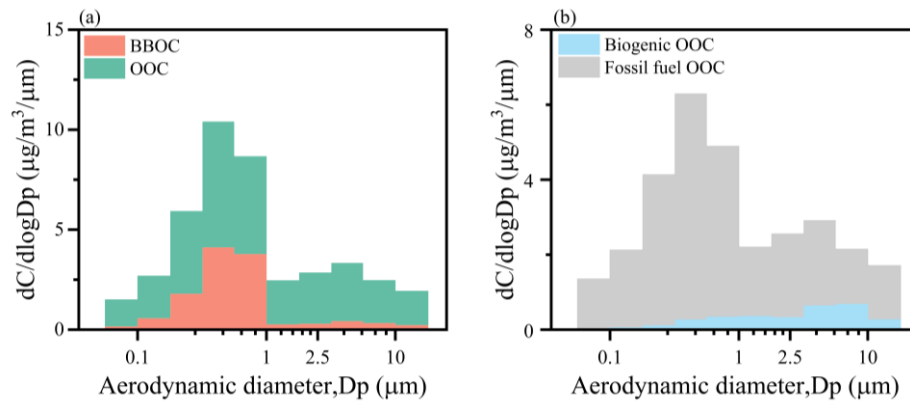


**Figure 3.** Average size distributions of the WSOC compositions, OOC and BBOC (a), fossil fuel OOC and biogenic OOC(b).

After removing the contributions from BBOC, the results clearly indicate that fossil fuel organic carbon (OOC) dominates in both fine (95.8%) and coarse (80.4%) modes, reflecting the significant role

of anthropogenic sources in SOA generation. Regarding particle size distribution, fossil fuel OOC is predominantly found in the fine mode (66.0%), while biogenic OOC is mainly present in the coarse mode (74.1%). This distribution indicates the differing reaction pathways for SOA in fine and coarse modes.

We further explore the relationship between fine- and coarse-mode OOC and gaseous precursors, more details of the gaseous precursors are provided in the supporting information (Table S2). We observed a high correlation between fine-mode OOC and polar carbonyl compounds, such as glyoxal, methylglyoxal, acetone, and MVK+MACR (Table 1). Carbonyl compounds are first- and/or second-generation gas-phase oxidation products of both anthropogenic (e.g., aromatics, acetylene) and biogenic (e.g., isoprene) sources (Ervens et al., 2011), this also suggests a complex source profile for fine mode SOA. Additionally, carbonyl compounds have strong water solubility and can be absorbed into clouds and fog to react with  $\cdot\text{OH}$  to form oligomers, which promote the formation of SOA (Wang et al., 2022). In contrast, coarse-mode OOC exhibited significant negative correlations with nonpolar aromatic hydrocarbons (e.g., toluene, C8 aromatic, C9 aromatic, styrene) and biogenic VOCs (monoterpenes) (Table 1). Despite these negative correlations, several evidence support atmospheric relevance of these gaseous precursors to coarse-mode SOA. Firstly, the correlations with aromatic and biogenic VOCs were unique to coarse-mode OOC and not observed in the fine-mode OOC, clearly demonstrating distinct precursor pathways for coarse and fine-mode SOA. Secondly,  $^{14}\text{C}$  isotope analysis explicitly confirmed that coarse-mode OOC consisted of both fossil (approximately 80.4%) and biogenic (approximately 19.6%) components, directly aligning with the respective aromatic and biogenic VOC precursors identified here. Thirdly, biogenic OOC was found predominantly in coarse-mode particles (74.1%), providing direct observational evidence linking biogenic VOC oxidation products to coarse-mode aerosol formation. This revealed different gaseous precursors for fine- and coarse-mode SOA, and reflected the different SOA

generation mechanisms that may exist.

**Table 1.** The correlation coefficients between OOC and typical VOCs in the campaign. \* indicates a significance level of 95% ( $p < 0.05$ ).

	Monoterpenes	Isoprene	MVK+MACR	Toluene	C8 aromatic	C9 aromatic	Styrene	Glyoxal	Methylglyoxal	Acetone
Fine mode OOC	0.20	0.47	0.70*	0.38	0.39	0.36	0.46	0.70*	0.73*	0.62*
Coarse mode OOC	-0.75*	-0.56	-0.34	-0.60*	-0.65*	-0.66*	-0.74*	-0.39	-0.39	-0.52

### 3.3 Possible formation mechanisms for fine mode SOA

The previous results reveal a distinct origin for fine and coarse mode OOC, suggesting different SOA generation mechanisms. Therefore, additional field measurements are necessary to further understand the mechanisms and key factors affecting SOA formation.

Building on the findings from the previous section that fine-mode OOC are primarily derived from carbonyl compounds, it is noteworthy that carbonyl compounds are highly reactive and exhibit significant water solubility (Liu et al., 2022; Wang et al., 2022; Xu et al., 2022). These properties enable them to contribute significantly to SOA formation through aqueous-phase reactions, particularly for dicarbonyls such as glyoxal (Gly, CHOCHO) and methylglyoxal (Mgly, CH<sub>3</sub>COCHO), which have been identified as key SOA precursors (Liu et al., 2022; Tan et al., 2017). Previous studies have identified characteristic fragment ions of glyoxal and methylglyoxal (e.g., C<sub>2</sub>O<sub>2</sub><sup>+</sup> and CH<sub>2</sub>O<sub>2</sub><sup>+</sup>), detected by aerosol mass spectrometer (AMS) and aerosol chemical speciation monitor (ACSM), which play a crucial role in the formation of low-volatility SOA during cloud processing and are strongly correlated with aqueous oxygenated organic aerosol (aq-OOA) (Duan et al., 2020; Sun et al., 2016). As shown in Figure 4a, these fragment ions are predominantly distributed in fine particles, indicating the significance of aqueous-phase processing in the fine mode. Further evidence of aqueous-phase reactions is provided by the behavior of MVK and MACR. While the direct aqueous-phase reaction of MVK and MACR with ozone

is less competitive compared to the faster OH-initiated reactions (Chen et al., 2008), aerosol liquid water content (ALWC) serves as a key metric for characterizing aqueous-phase SOA formation due to its positive correlation with these processes, especially under conditions of high relative humidity and elevated NO<sub>x</sub> levels (Kuang et al., 2020b; McNeill, 2015; Zhan et al., 2021). In this study, we observed a strong positive correlation between fine-mode OOC and ALWC (Figure 4b), suggesting that fine-mode SOA is predominantly generated through aqueous-phase processes.

However, in contrast to the coarse mode, in contrast to the coarse modes, the fine modes are not abundant in ALWC (Figure S6). Despite this, we observed a significant relationship between OOC and ALWC exclusively in the fine mode. To further investigate the behavior of carbonyl compounds under the unique conditions of the fine mode, we analyzed the correlations of fine- and coarse-mode OOC with key factors, revealing notable differences between the two modes. First, the fine mode is characterized by higher concentrations of inorganic ions, such as sulfate and nitrate, which may play a critical role in SOA formation. Specifically, sulfate demonstrated a stronger positive influence on fine-mode OOC formation compared to nitrate, as evidenced by their respective correlation coefficients ( $R^2 = 0.85$  for sulfate, Figure 4c;  $R^2 = 0.47$  for nitrate, Figure 4d). This discrepancy may arise from the fact that sulfate ( $\text{SO}_4^{2-}$ ) is primarily produced through aqueous-phase reactions, whereas nitrate ( $\text{NO}_3^-$ ) is predominantly generated via gas-phase reactions (Zhan et al., 2021). Additionally, the fine mode exhibits acidic conditions ( $\text{pH}_{\text{aerosol}} = 0.4\text{--}4.3$ ), and we observed distinct correlations between fine-mode OOC and  $\text{pH}_{\text{aerosol}}$  (Figure 4e). This suggests that the lower pH in the fine mode favors the formation of fine-mode OOC.

A few studies have emphasized the significant role of metal ions in SOA formation, particularly under low pH conditions. To further investigate this, we examined the correlation between water-soluble metal

ions and fine-mode OOC (Table S5). Our analysis revealed that fine-mode OOC exhibits a strong correlation with water-soluble Fe ions ( $r = 0.82$ ,  $p < 0.05$ ), and a positive relationship was observed between the concentration of iron ions and fine-mode OOC (Figure 5f). Additionally, water-soluble iron ions were found to be highly concentrated in the fine mode (Figure S4), with their concentration ( $18.87 \text{ ng/m}^3$ ) significantly exceeding that of other metal ions. Recent studies have highlighted the role of water-soluble Fe ions in Fenton chemistry, where they cycle between  $\text{Fe}^{2+}$  and  $\text{Fe}^{3+}$ . This process, particularly through Fenton reactions involving peroxides, may substantially enhance SOA formation by supplying particle-phase oxidants (Qin et al., 2022; Ye et al., 2021). Specifically, Fenton reactions within aqueous particles can generate hydroxyl radicals ( $\text{OH}$ ), which oxidize organic compounds such as carbonyls, especially under lower pH conditions (Kuang et al., 2020a).

Therefore, in this study, we propose that aqueous-phase reactions play a dominant role in the formation of fine-mode SOA. The lower pH and elevated concentrations of water-soluble Fe ions in the fine mode create favorable conditions for SOA formation from carbonyl compounds, primarily through Fenton reactions.

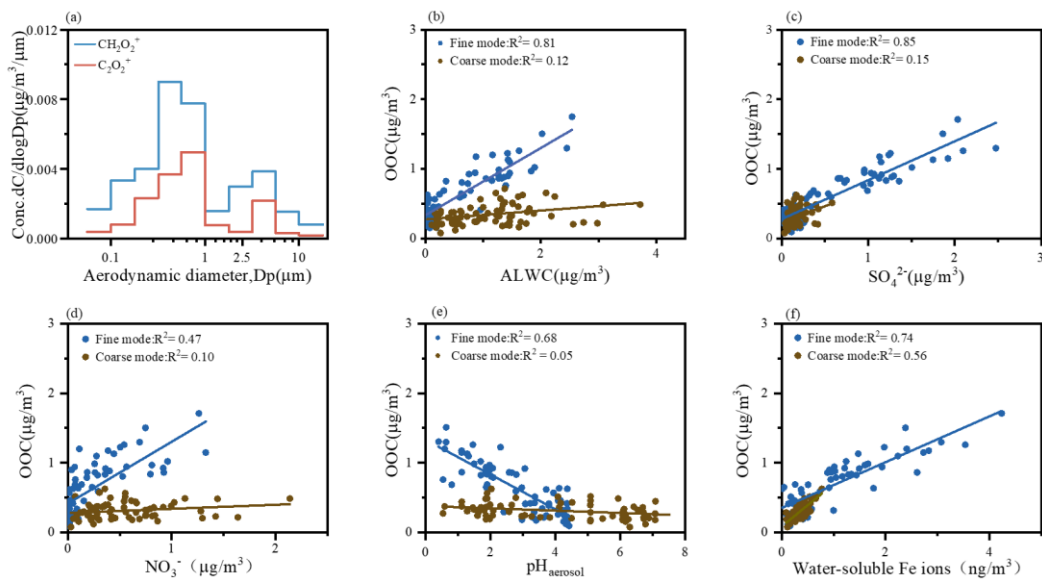


**Figure 4.** Average size distributions of  $\text{CH}_2\text{O}_2^+$  and  $\text{C}_2\text{O}_2^+$  (a), and relationship between OOC and ALWC (b),  $\text{SO}_4^{2-}$  (c),  $\text{NO}_3^-$  (d),  $\text{pH}_{\text{aerosol}}$  (e), water-soluble iron ions (f)

### 3.4 Possible formation mechanisms for coarse mode SOA

Most previous studies have focused on the heterogeneous uptake of inorganic trace gases by coarse particles, while the interaction between VOCs and coarse particles remains largely unexplored. Consequently, the role of coarse particles in SOA formation and growth under typical polluted urban conditions is still poorly understood (Yu et al., 2016; Yu and Jang, 2019).

A distinct phenomenon observed in our experiments is that biogenic-OOC are predominantly distributed in the coarse mode, which may be attributed to unique SOA formation pathways in this mode. Biogenic-OOC is primarily generated through the oxidation of BVOCs by atmospheric oxidants such as hydroxyl radicals (OH), ozone ( $\text{O}_3$ ), and nitrate radicals ( $\text{NO}_3$ ) (Gagan et al., 2023). BVOCs emitted by terrestrial vegetation, including isoprene and monoterpenes, significantly contribute to the total SOA budget. As shown in Table 1, coarse-mode OOC exhibits a strong correlation with monoterpenes ( $r = -0.75$ ,  $p < 0.05$ ) but a weaker correlation with isoprene ( $r = -0.56$ ,  $p < 0.05$ ), suggesting that monoterpenes play a more prominent role in biogenic-OOC formation.



Regarding the mechanisms of SOA generation from monoterpenes and isoprene, isoprene primarily reacts with OH radicals to form SOA, whereas monoterpenes, in addition to reacting with OH radicals, also undergo significant SOA formation through reactions with O<sub>3</sub> (McFiggans et al., 2019; Xu et al., 2015). Previous studies have demonstrated that monoterpene-derived SOA is more oxidized in the presence of nitrate-containing seed aerosols compared to ammonium sulfate seed aerosols (Huang et al., 2016; Watne et al., 2017). The higher nitrate concentrations in the coarse mode further favor the O<sub>3</sub> oxidation pathway for monoterpenes. Our sampling site, located in the PRD region, is one of the most rapidly urbanized areas with high anthropogenic emissions (Ma et al., 2024). The sampling period coincided with elevated O<sub>3</sub> pollution levels. Coarse-mode particles, characterized by higher pH compared to fine-mode particles, create conditions conducive to photosensitive reactions and O<sub>3</sub> oxidation pathways (Yu and Jang, 2019). Further analysis reveals a strong correlation between coarse-mode OOC and O<sub>3</sub> (Figure 5a). Additionally, Figure 5b demonstrates that coarse-mode OOC concentrations are significantly higher during high-O<sub>3</sub> periods compared to low-O<sub>3</sub> periods, with a distinct peak observed during high-O<sub>3</sub> episodes. Notably, no significant increase in the concentrations of other inorganic ions was observed during these high-O<sub>3</sub> periods (Figure S6). These findings collectively underscore the critical role of O<sub>3</sub> in the formation of coarse-mode SOA.

However, the reaction pathways involved in coarse-mode secondary organic aerosol (SOA) formation remain poorly understood. The <sup>14</sup>C isotope analysis results indicate that fossil fuel-derived oxygenated organic compounds (OOC) are the primary source of coarse-mode OOC. Additionally, coarse-mode OOC exhibits a stronger correlation with aromatic VOCs, particularly styrene (Table 1). However, since nonpolar aromatic hydrocarbons do not directly react with O<sub>3</sub> to form SOA, further investigation is needed to elucidate the role of O<sub>3</sub> in coarse-mode SOA formation. Recent studies have highlighted the

rapid gas-phase autoxidation of endocyclic alkenes initiated by ozonolysis, which yields highly oxygenated organic molecules (HOMs), particularly from monoterpenes and aromatic compounds (Rissanen, 2021). Chemistry transport models have demonstrated that ozonolysis of monoterpenes accounts for 79% of HOMs production (Shi et al., 2021). Additionally, photochemical oxidation of substituted aromatic compounds has been shown to form HOMs through rapid intramolecular autoxidation reactions, a process analogous to the oxidation of monoterpenes. O<sub>3</sub> can facilitate these reactions during the photo-oxidation of aromatics (Molteni et al., 2018; Suh et al., 2003; Wang et al., 2020a), which partially explains the stronger correlation between O<sub>3</sub> and coarse-mode OOC. This conclusion is further supported by the higher oxidation state (O/C ratio) observed in the coarse mode compared to the fine mode (Figure 5c).

Moreover, recent studies have identified carboxylic acids as products of these reactions (Zhang et al., 2017a). The slope of coarse-mode OOC in the Van Krevelen (VK) plot is close to -0.5 (Figure 5d), indicating the large formation of carboxylic acids with fragmentation through the replacement of hydrogen atoms. The coarse mode is characterized by higher ALWC, higher pH, and favorable partitioning of reaction products into the particulate phase. Based on these findings, we propose that gas-phase autoxidation plays a significant role in the formation of coarse-mode SOA.

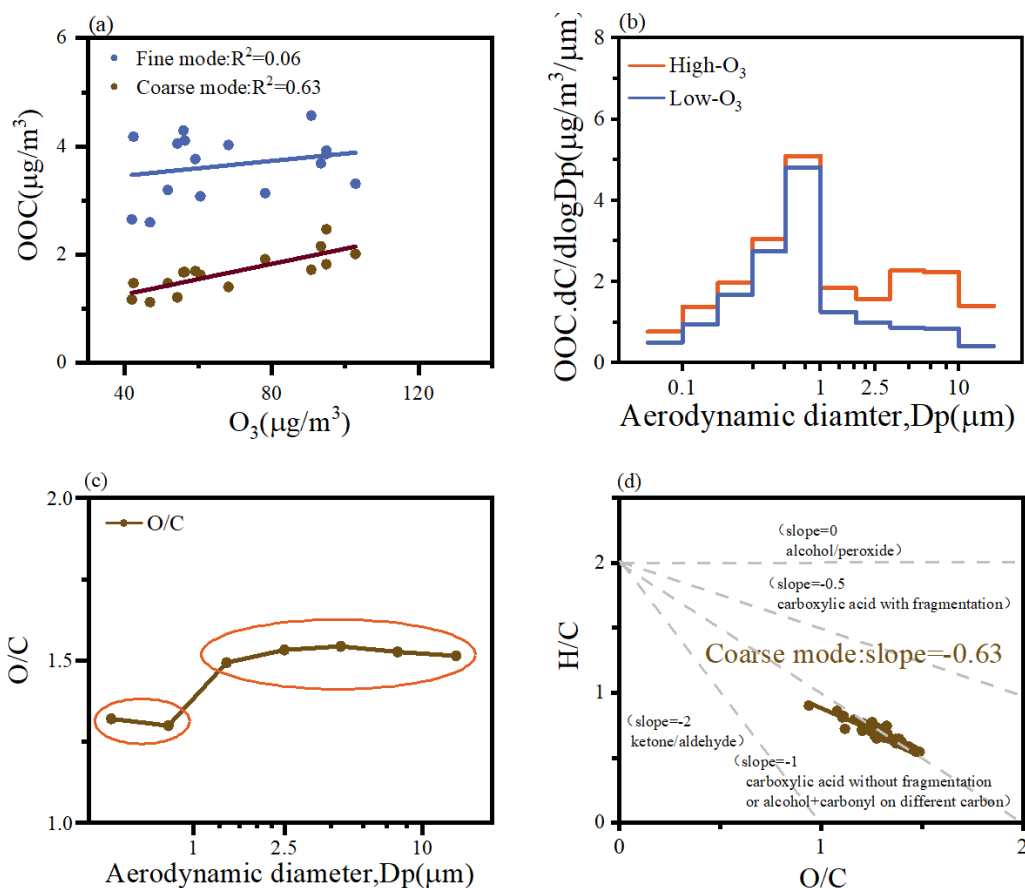


**Figure 5.** Relationship between OOC and O<sub>3</sub> (a) , average size distributions of OOC (b), and organic O/C(c), Van Krevelen diagram of H / C vs. O / C(d).

#### 4 Summary and implications

This study collected 16 sets of size-segregated aerosol samples (0.056–18 μm) in Shenzhen, a coastal city in the Pearl River Delta, from October 2022 to January 2023. The water-soluble components, including typical inorganic ions, water-soluble organic compounds, and water-soluble metal ions, were analyzed, and WSOM emerged as the most abundant water-soluble component in both modes, accounting for 55.9% and 40.9% of the total water-soluble mass in fine and coarse particles, respectively. This highlights the critical role of WSOM in both size fractions.

Our findings indicate that WSOM in both fine and coarse modes exhibits secondary production. To

quantify secondary organic aerosol (SOA), which is represented by oxygenated organic carbon (OOC), we applied Positive Matrix Factorization (PMF) modeling and utilized radiocarbon isotopes to distinguish between fossil fuel-derived and biogenic organic carbon (OOC). Radiocarbon ( $^{14}\text{C}$ ) isotope analysis reveals that fossil sources dominate SOA in both fine (95.8%) and coarse (80.4%) modes, while the small amount of biogenic SOA mostly existed in the coarse mode (74.1%), we emphasize the significant contribution of anthropogenic volatile organic compounds (VOCs) to SOA formation in coastal atmospheres, where high relative humidity and enhanced atmospheric oxidation capacity also play pivotal roles in SOA generation across both fine and coarse modes. Furthermore, we investigated potential precursor sources for fine- and coarse-mode OOC, fine-mode oxygenated organic carbon (OOC) correlates strongly with polar carbonyl compounds (e.g., glyoxal, methylglyoxal, acetone, and MVK+MACR), while coarse-mode OOC exhibits better correlations with nonpolar aromatic hydrocarbons (e.g., toluene, C8 aromatic, C9 aromatic, styrene) and biogenic VOCs (e.g., monoterpenes, isoprene), indicating that the sources of fine- and coarse-mode OOC are different, indicating that the sources of fine- and coarse-mode OOC are different, indicating distinct precursor sources for SOA in different size modes.

Multivariate analyses incorporating inorganic ions, pH, water-soluble Fe ions, aerosol liquid water content, and  $\text{O}_3$  revealed divergent size-dependent mechanisms, emphasizing the significant role of aqueous-phase reactions in fine-mode OOC formation, particularly the key contribution of water-soluble iron ions ( $r^2 = 0.74$ ), while coarse-mode OOC exhibited a notable correlation with  $\text{O}_3$  ( $r^2 = 0.63$ ). Combining the information on VOCs precursors and key components, our study elucidates that aqueous-phase reactions play a key role in fine-mode OOC, especially the Fenton reaction, while gas-phase autoxidation plays an important role in the coarse-mode OOC generation. By examining OOC formation

across a wide range of particle sizes, this study provides novel insights into SOA formation mechanisms and enhances our understanding of the formation pathways of SOA in both fine and coarse mode. However, the specific mechanisms governing SOA generation in different particle size ranges remain poorly understood. We strongly recommend further laboratory experiments to explore these mechanisms in greater depth. Notably, our study underscores the significant role of anthropogenic VOCs in SOA formation in coastal environments, where high relative humidity and atmospheric oxidation capacity are critical drivers. Similar conditions are prevalent in marginal seas and estuaries near urban areas, warranting further in-depth studies in these representative regions.

**Data availability.** Datasets are available by contacting the corresponding author, Meng-Xue Tang

([tangmx@pku.edu.cn](mailto:tangmx@pku.edu.cn))

**Supplement.** The supplement material related to this article is available online at:

**Author contributions.** J.-Y.W., M.-X.T., and X.-F.H. conceptualized the study. J.-Y.W., S.L., and K.-J.T. executed the experiments. J.-Y.W., M.-X.T., and X.P. carried out the statistical analysis. J.-Y.W. prepared the first draft of the manuscript, which was commented on and revised by M.-X.T., L.-Y.H., and X.-F.H. All authors reviewed and approved the final version for publication.

**Competing interests.** The authors declare that they have no conflict of interest.

**Financial support.** This work was supported by the National Key Research and Development Program of China (2022YFC3701000, Task2) and the National Natural Science Foundation of China (42407145).

## Reference

- Boreddy, S. K. R. and Kawamura, K.: A 12-year observation of water-soluble ions in TSP aerosols collected at a remote marine location in the western North Pacific: an outflow region of Asian dust, *Atmospheric Chem. Phys.*, 15, 6437–6453, 2015.
- Chen, Z. M., Wang, H. L., Zhu, L. H., Wang, C. X., Jie, C. Y., and Hua, W.: Aqueous-phase ozonolysis of methacrolein and methyl vinyl ketone: a potentially important source of atmospheric aqueous oxidants, *Atmos Chem Phys*, 2008.
- Dominutti, P. A., Chevassus, E., Baray, J.-L., Jaffrezo, J.-L., Borbon, A., Colomb, A., Deguillaume, L., El Gdachi, S., Houdier, S., Leriche, M., Metzger, J.-M., Rocco, M., Tulet, P., Sellegri, K., and Freney, E.: Evaluation of the Sources, Precursors, and Processing of Aerosols at a High-Altitude Tropical Site, *ACS Earth Space Chem.*, 6, 2412–2431, 2022.
- Duan, J., Huang, R.-J., Li, Y., Chen, Q., Zheng, Y., Chen, Y., Lin, C., Ni, H., Wang, M., Ovadnevaite, J., Ceburnis, D., Chen, C., Worsnop, D. R., Hoffmann, T., O'Dowd, C., and Cao, J.: Summertime and wintertime atmospheric processes of secondary aerosol in Beijing, *Atmospheric Chem. Phys.*, 20, 3793–3807, 2020.
- Ervens, B., Turpin, B. J., and Weber, R. J.: Secondary organic aerosol formation in cloud droplets and aqueous particles (aqSOA): a review of laboratory, field and model studies, *Atmospheric Chem. Phys.*, 11, 11069–11102, 2011.
- Gagan, S., Sarang, K., Rudzinski, K. J., Liu, R., Szmigielski, R., and Zhang, Y.: Synthetic strategies for oxidation products from biogenic volatile organic compounds in the atmosphere: A review, *Atmos. Environ.*, 312, 120017, 2023.
- George, C., Ammann, M., D'Anna, B., Donaldson, D. J., and Nizkorodov, S. A.: Heterogeneous Photochemistry in the Atmosphere, *Chem. Rev.*, 115, 4218–4258, 2015.
- Gu, Y., Huang, R.-J., Duan, J., Xu, W., Lin, C., Zhong, H., Wang, Y., Ni, H., Liu, Q., Xu, R., Wang, L., and Li, Y. J.: Multiple pathways for the formation of secondary organic aerosol in the North China Plain in summer, *Atmospheric Chem. Phys.*, 23, 5419–5433, 2023.
- Hallquist, M., Wenger, J. C., Baltensperger, U., Rudich, Y., Simpson, D., Claeys, M., Dommen, J., Donahue, N. M., George, C., Goldstein, A. H., Hamilton, J. F., Herrmann, H., Hoffmann, T., Iinuma, Y., Jang, M., Jenkin, M. E., Jimenez, J. L., Kiendler-Scharr, A., Maenhaut, W., McFiggans, G., Mentel, T. F., Monod, A., Prévôt, A. S. H., Seinfeld, J. H., Surratt, J. D., Szmigielski, R., and Wildt, J.: The formation, properties and impact of secondary organic aerosol: current and emerging issues, *Atmospheric Chem. Phys.*, 9, 5155–5236, 2009.
- He, D.-Y., Huang, X.-F., Wei, J., Wei, F.-H., Zhu, B., Cao, L.-M., and He, L.-Y.: Soil dust as a potential bridge from biogenic volatile organic compounds to secondary

409 organic aerosol in a rural environment, *Environ. Pollut.*, 298, 118840, 2022a.

410 He, D.-Y., Huang, X.-F., Wei, J., Wei, F.-H., Zhu, B., Cao, L.-M., and He, L.-Y.: Soil  
 411 dust as a potential bridge from biogenic volatile organic compounds to secondary  
 412 organic aerosol in a rural environment, *Environ. Pollut.*, 298, 118840, 2022b.

413 Huang, D. D., Zhang, X., Dalleska, N. F., Lignell, H., Coggon, M. M., Chan, C., Flagan,  
 414 R. C., Seinfeld, J. H., and Chan, C. K.: A note on the effects of inorganic seed aerosol  
 415 on the oxidation state of secondary organic aerosol— $\alpha$ -Pinene ozonolysis, *J. Geophys.*  
 416 *Res. Atmospheres*, 121, 2016.

417 Huang, X.-F., Dai, J., Zhu, Q., Yu, K., and Du, K.: Abundant Biogenic Oxygenated  
 418 Organic Aerosol in Atmospheric Coarse Particles: Plausible Sources and Atmospheric  
 419 Implications, *Environ. Sci. Technol.*, 54, 1425–1430, 2020.

420 Jimenez, J. L., Canagaratna, M. R., Donahue, N. M., Prevot, A. S. H., Zhang, Q., Kroll,  
 421 J. H., DeCarlo, P. F., Allan, J. D., Coe, H., Ng, N. L., Aiken, A. C., Docherty, K. S.,  
 422 Ulbrich, I. M., Grieshop, A. P., Robinson, A. L., Duplissy, J., Smith, J. D., Wilson, K.  
 423 R., Lanz, V. A., Hueglin, C., Sun, Y. L., Tian, J., Laaksonen, A., Raatikainen, T.,  
 424 Rautiainen, J., Vaattovaara, P., Ehn, M., Kulmala, M., Tomlinson, J. M., Collins, D. R.,  
 425 Cubison, M. J., E., Dunlea, J., Huffman, J. A., Onasch, T. B., Alfarra, M. R., Williams,  
 426 P. I., Bower, K., Kondo, Y., Schneider, J., Drewnick, F., Borrmann, S., Weimer, S.,  
 427 Demerjian, K., Salcedo, D., Cottrell, L., Griffin, R., Takami, A., Miyoshi, T.,  
 428 Hatakeyama, S., Shimono, A., Sun, J. Y., Zhang, Y. M., Dzepina, K., Kimmel, J. R.,  
 429 Sueper, D., Jayne, J. T., Herndon, S. C., Trimborn, A. M., Williams, L. R., Wood, E.  
 430 C., Middlebrook, A. M., Kolb, C. E., Baltensperger, U., and Worsnop, D. R.: Evolution  
 431 of Organic Aerosols in the Atmosphere, *Science*, 326, 1525–1529,  
 432 <https://doi.org/10.1126/science.1180353>, 2009.

433 Klopper, D., Formenti, P., Namwoonde, A., Cazaunau, M., Chevaillier, S., Feron, A.,  
 434 Gaimoz, C., Hease, P., Lahmidi, F., Mirande-Bret, C., Triquet, S., Zeng, Z., and Piketh,  
 435 S. J.: Chemical composition and source apportionment of atmospheric aerosols on the  
 436 Namibian coast, *Atmos Chem Phys*, 2020.

437 Kuang, X. M., Gonzalez, D. H., Scott, J. A., Vu, K., Hasson, A., Charbouillot, T.,  
 438 Hawkins, L., and Paulson, S. E.: Cloud Water Chemistry Associated with Urban  
 439 Aerosols: Rapid Hydroxyl Radical Formation, Soluble Metals, Fe(II), Fe(III), and  
 440 Quinones, *ACS Earth Space Chem.*, 4, 67–76, 2020a.

441 Kuang, Y., He, Y., Xu, W., Yuan, B., Zhang, G., Ma, Z., Wu, C., Wang, C., Wang, S.,  
 442 Zhang, S., Tao, J., Ma, N., Su, H., Cheng, Y., Shao, M., and Sun, Y.: Photochemical  
 443 Aqueous-Phase Reactions Induce Rapid Daytime Formation of Oxygenated Organic  
 444 Aerosol on the North China Plain, *Environ. Sci. Technol.*, 54, 3849–3860, 2020b.

445 Li, W. J. and Shao, L. Y.: Observation of nitrate coatings on atmospheric mineral dust  
 446 particles, *Atmos Chem Phys*, 2009.



447 Li, Z.-J., He, L.-Y., Ma, H.-N., Peng, X., Tang, M.-X., Du, K., and Huang, X.-F.:  
 448 Sources of atmospheric oxygenated volatile organic compounds in different air masses  
 449 in Shenzhen, China, *Environ. Pollut.*, 340, 122871, 2024a.

450 Li, Z.-J., He, L.-Y., Ma, H.-N., Peng, X., Tang, M.-X., Du, K., and Huang, X.-F.:  
 451 Sources of atmospheric oxygenated volatile organic compounds in different air masses  
 452 in Shenzhen, China, *Environ. Pollut.*, 340, 122871, 2024b.

453 Liu, Q., Gao, Y., Huang, W., Ling, Z., Wang, Z., and Wang, X.: Carbonyl compounds  
 454 in the atmosphere: A review of abundance, source and their contributions to O<sub>3</sub> and  
 455 SOA formation, *Atmospheric Res.*, 274, 106184, 2022.

456 Ma, F., Wang, H., Ding, Y., Zhang, S., Wu, G., Li, Y., Gong, D., Ristovski, Z., He, C.,  
 457 and Wang, B.: Amplified Secondary Organic Aerosol Formation Induced by  
 458 Anthropogenic–Biogenic Interactions in Forests Around Megacities, *J. Geophys. Res.*  
 459 *Atmospheres*, 129, e2024JD041679, 2024.

460 McFiggans, G., Mentel, T. F., Wildt, J., Pullinen, I., Kang, S., Kleist, E., Schmitt, S.,  
 461 Springer, M., Tillmann, R., Wu, C., Zhao, D., Hallquist, M., Faxon, C., Le Breton, M.,  
 462 Hallquist, Å. M., Simpson, D., Bergström, R., Jenkin, M. E., Ehn, M., Thornton, J. A.,  
 463 Alfarra, M. R., Bannan, T. J., Percival, C. J., Priestley, M., Topping, D., and Kiendler-  
 464 Scharr, A.: Secondary organic aerosol reduced by mixture of atmospheric vapours,  
 465 *Nature*, 565, 587–593, 2019.

466 McNeill, V. F.: Aqueous Organic Chemistry in the Atmosphere: Sources and Chemical  
 467 Processing of Organic Aerosols, *Environ. Sci. Technol.*, 49, 1237–1244, 2015.

468 Mei, S., Xia, K., Liu, C., Chen, X., Yuan, R., Liu, H., Zhao, C., and Liu, S.: Aqueous-  
 469 Phase Processing Affects the Formation and Size Distribution of Aerosol Organic  
 470 Functional Groups During Heavy Pollution, *J. Geophys. Res. Atmospheres*, 130,  
 471 e2024JD042029, 2025.

472 Molteni, U., Bianchi, F., Klein, F., El Haddad, I., Frege, C., Rossi, M. J., Dommen, J.,  
 473 and Baltensperger, U.: Formation of highly oxygenated organic molecules from  
 474 aromatic compounds, *Atmospheric Chem. Phys.*, 18, 1909–1921, 2018.

475 Pan, Y., Quan, J., Ma, P., Liao, Z., Jia, X., Dou, Y., Cheng, Z., Lei, L., Wang, Y., Zheng,  
 476 M., Lü, D., and Wang, Y.: Mineral dust scavenges anthropogenic aerosols in polluted  
 477 environment, *Atmos. Environ.*, 309, 119938, 2023.

478 Peng, J., Hu, M., Shang, D., Wu, Z., Du, Z., Tan, T., Wang, Y., Zhang, F., and Zhang,  
 479 R.: Explosive Secondary Aerosol Formation during Severe Haze in the North China  
 480 Plain, *Environ. Sci. Technol.*, 55, 2189–2207, 2021.

481 Qin, X., Chen, Z., Gong, Y., Dong, P., Cao, Z., Hu, J., and Xu, J.: Persistent Uptake of  
 482 H<sub>2</sub> O<sub>2</sub> onto Ambient PM<sub>2.5</sub> via Dark-Fenton Chemistry, *Environ. Sci. Technol.*, 56,  
 483 9978–9987, 2022.

484 Rissanen, M.: Anthropogenic Volatile Organic Compound (AVOC) Autoxidation as a  
 485 Source of Highly Oxygenated Organic Molecules (HOM), *J. Phys. Chem. A*, 125,  
 486 9027–9039, 2021.

487 Shi, X., Huang, G., Yang, D., Zhang, Q., Zong, W., Cheng, J., Sui, X., Yuan, F., and  
 488 Wang, W.: Theoretical study of the formation and nucleation mechanism of highly  
 489 oxygenated multi-functional organic compounds produced by  $\alpha$ -pinene, *Sci. Total*  
 490 *Environ.*, 780, 146422, 2021.

491 Suh, I., Zhang, R., Molina, L. T., and Molina, M. J.: Oxidation Mechanism of Aromatic  
 492 Peroxy and Bicyclic Radicals from OH-Toluene Reactions, *J. Am. Chem. Soc.*, 125,  
 493 12655–12665, 2003.

494 Sun, Y., Du, W., Fu, P., Wang, Q., Li, J., Ge, X., Zhang, Q., Zhu, C., Ren, L., Xu, W.,  
 495 Zhao, J., Han, T., Worsnop, D. R., and Wang, Z.: Primary and secondary aerosols in  
 496 Beijing in winter: sources, variations and processes, *Atmospheric Chem. Phys.*, 16,  
 497 8309–8329, 2016.

498 Tan, H., Cai, M., Fan, Q., Liu, L., Li, F., Chan, P. W., Deng, X., and Wu, D.: An analysis  
 499 of aerosol liquid water content and related impact factors in Pearl River Delta, *Sci. Total*  
 500 *Environ.*, 579, 1822–1830, 2017.

501 Wang, J., Chen, S., Qiu, X., Niu, W., Li, O., Zhu, C., Zhang, X., Yang, X., and Zhang,  
 502 G.: Pollution Characteristics of Atmospheric Carbonyl Compounds in a Large City of  
 503 Northern China, *J. Chem.*, 2022, 1–13, 2022.

504 Wang, S., Newland, M. J., Deng, W., Rickard, A. R., Hamilton, J. F., Muñoz, A.,  
 505 Ródenas, M., Vázquez, M. M., Wang, L., and Wang, X.: Aromatic Photo-oxidation, A  
 506 New Source of Atmospheric Acidity, *Env. Sci Technol*, 2020a.

507 Wang, T., Liu, Y., Deng, Y., Cheng, H., Yang, Y., Feng, Y., Zhang, L., Fu, H., and  
 508 Chen, J.: Photochemical Oxidation of Water-Soluble Organic Carbon (WSOC) on  
 509 Mineral Dust and Enhanced Organic Ammonium Formation, *Environ. Sci. Technol.*,  
 510 54, 15631–15642, 2020b.

511 Watne, Å. K., Westerlund, J., Hallquist, Å. M., Brune, W. H., and Hallquist, M.: Ozone  
 512 and OH-induced oxidation of monoterpenes: Changes in the thermal properties of  
 513 secondary organic aerosol (SOA), *J. Aerosol Sci.*, 114, 31–41, 2017.

514 Wu, X., Kong, Q., Lan, Y., Sng, J., and Yu, L. E.: Refined Sea Salt Markers for Coastal  
 515 Cities Facilitating Quantification of Aerosol Aging and PM<sub>2.5</sub> Apportionment, *Environ.*  
 516 *Sci. Technol.*, 2024.

517 Xu, B., Zhang, G., Gustafsson, Ö., Kawamura, K., Li, J., Andersson, A., Bikkina, S.,  
 518 Kunwar, B., Pokhrel, A., Zhong, G., Zhao, S., Li, J., Huang, C., Cheng, Z., Zhu, S.,  
 519 Peng, P., and Sheng, G.: Large contribution of fossil-derived components to aqueous  
 520 secondary organic aerosols in China, *Nat. Commun.*, 13, 5115, 2022.

- 521 Xu, L., Guo, H., Boyd, C. M., Klein, M., Bougiatioti, A., Cerully, K. M., Hite, J. R.,  
522 Isaacman-VanWertz, G., Kreisberg, N. M., Knote, C., Olson, K., Koss, A., Goldstein,  
523 A. H., Hering, S. V., De Gouw, J., Baumann, K., Lee, S.-H., Nenes, A., Weber, R. J.,  
524 and Ng, N. L.: Effects of anthropogenic emissions on aerosol formation from isoprene  
525 and monoterpenes in the southeastern United States, *Proc. Natl. Acad. Sci.*, 112, 37–42,  
526 2015.
- 527 Xu, M., Hu, B., Zhao, S., Yan, G., Wen, T., and Zhao, X.: Size-resolved water-soluble  
528 organic carbon and its significant contribution to aerosol liquid water, *Sci. Total*  
529 *Environ.*, 927, 172396, 2024.
- 530 Xu, W., Han, T., Du, W., Wang, Q., Chen, C., Zhao, J., Zhang, Y., Li, J., Fu, P., Wang,  
531 Z., Worsnop, D. R., and Sun, Y.: Effects of Aqueous-Phase and Photochemical  
532 Processing on Secondary Organic Aerosol Formation and Evolution in Beijing, China,  
533 *Environ. Sci. Technol.*, 51, 762–770, 2017.
- 534 Yang, W., Ma, J., Yang, H., Li, F., and Han, C.: Photoenhanced sulfate formation by  
535 the heterogeneous uptake of SO<sub>2</sub> on non-photoactive mineral dust, *Atmospheric Chem.*  
536 *Phys.*, 24, 6757–6768, 2024.
- 537 Yao, D., Guo, H., Lyu, X., Lu, H., and Huo, Y.: Secondary organic aerosol formation  
538 at an urban background site on the coastline of South China: Precursors and aging  
539 processes, *Environ. Pollut.*, 309, 119778, 2022.
- 540 Ye, C., Chen, H., Hoffmann, E. H., Mettke, P., Tilgner, A., He, L., Mutzel, A.,  
541 Brüggemann, M., Poulain, L., Schaefer, T., Heinold, B., Ma, Z., Liu, P., Xue, C., Zhao,  
542 X., Zhang, C., Zhang, F., Sun, H., Li, Q., Wang, L., Yang, X., Wang, J., Liu, C., Xing,  
543 C., Mu, Y., Chen, J., and Herrmann, H.: Particle-Phase Photoreactions of HULIS and  
544 TMIs Establish a Strong Source of H<sub>2</sub> O<sub>2</sub> and Particulate Sulfate in the Winter North  
545 China Plain, *Environ. Sci. Technol.*, 55, 7818–7830, 2021.
- 546 Yu, G.-H., Park, S., and Lee, K.-H.: Source contributions and potential source regions  
547 of size-resolved water-soluble organic carbon measured at an urban site over one year,  
548 *Environ. Sci. Process. Impacts*, 18, 1343–1358, 2016.
- 549 Yu, Z. and Jang, M.: Atmospheric Processes of Aromatic Hydrocarbons in the Presence  
550 of Mineral Dust Particles in an Urban Environment, *ACS Earth Space Chem.*, 2019.
- 551 Zhan, B., Zhong, H., Chen, H., Chen, Y., Li, X., Wang, L., Wang, X., Mu, Y., Huang,  
552 R.-J., George, C., and Chen, J.: The roles of aqueous-phase chemistry and  
553 photochemical oxidation in oxygenated organic aerosols formation, *Atmos. Environ.*,  
554 266, 118738, 2021.
- 555 Zhang, X., Lambe, A. T., Upshur, M. A., Brooks, W. A., Gray Bé, A., Thomson, R. J.,  
556 Geiger, F. M., Surratt, J. D., Zhang, Z., Gold, A., Graf, S., Cubison, M. J., Groessl, M.,  
557 Jayne, J. T., Worsnop, D. R., and Canagaratna, M. R.: Highly Oxygenated

558 Multifunctional Compounds in  $\alpha$ -Pinene Secondary Organic Aerosol, Environ. Sci.  
559 Technol., 51, 5932–5940, 2017a.

560 Zhang, X., Li, J., Mo, Y., Shen, C., Ding, P., Wang, N., Zhu, S., Cheng, Z., He, J., Tian,  
561 Y., Gao, S., Zhou, Q., Tian, C., Chen, Y., and Zhang, G.: Isolation and radiocarbon  
562 analysis of elemental carbon in atmospheric aerosols using hydropyrolysis, Atmos.  
563 Environ., 198, 381–386, 2019.

564 Zhang, Y., Cai, J., Wang, S., He, K., and Zheng, M.: Review of receptor-based source  
565 apportionment research of fine particulate matter and its challenges in China, Sci. Total  
566 Environ., 586, 917–929, 2017b.

567